*Cerebral Cortex*, 2019;00: 1–17

**doi: 10.1093/cercor/bhz247**
Advance Access Publication Date:
Original Article



ORIGINAL ARTICLE

# Functional Territories of Human Dentate Nucleus

Xavier Guell[1,2], Anila M. D'Mello[1], Nicholas A. Hubbard[1,3], Rachel R. Romeo[1,4], John D. E. Gabrieli[1], Susan Whitfield-Gabrieli[1,5], Jeremy D. Schmahmann[2] and Sheeba Arnold Anteraper[1,5]

[1]McGovern Institute for Brain Research, Massachusetts Institute of Technology, Cambridge, MA 02139, USA, [2]Ataxia Unit, Cognitive Behavioral Neurology Unit, Laboratory for Neuroanatomy and Cerebellar Neurobiology, Department of Neurology, Massachusetts General Hospital, Harvard Medical School, Boston, MA 02114, USA, [3]University of Nebraska, Lincoln, Center for Brain, Biology, and Behavior, Department of Psychology, Lincoln, NE 68588, USA, [4]Boston Children's Hospital, Division of Developmental Medicine, Boston, MA 02115, USA, and [5]Department of Psychology, Northeastern University, Boston, MA 02115, USA

Address correspondence to Xavier Guell, Massachusetts Institute of Technology, McGovern Institute for Brain Research, Cambridge, MA 02139, USA. Email: xaviergp@mit.edu.

## Abstract

Anatomical connections link the cerebellar cortex with multiple sensory, motor, association, and paralimbic cerebral areas. The majority of fibers that exit cerebellar cortex synapse in dentate nuclei (DN) before reaching extracerebellar structures such as cerebral cortex, but the functional neuroanatomy of human DN remains largely unmapped. Neuroimaging research has redefined broad categories of functional division in the human brain showing that primary processing, attentional (task positive) processing, and default-mode (task negative) processing are three central poles of neural macroscale functional organization. This broad spectrum of human neural processing categories is represented not only in the cerebral cortex, but also in the thalamus, striatum, and cerebellar cortex. Whether functional organization in DN obeys a similar set of macroscale divisions, and whether DN are yet another compartment of representation of a broad spectrum of human neural processing categories, remains unknown. Here, we show for the first time that human DN are optimally divided into three functional territories as indexed by high spatio-temporal resolution resting-state MRI in 77 healthy humans, and that these three distinct territories contribute uniquely to default-mode, salience-motor, and visual cerebral cortical networks. Our findings provide a systems neuroscience substrate for cerebellar output to influence multiple broad categories of neural control.

**Key words:** cerebellum, default mode network, functional gradients, fMRI, salience network

## Introduction

Neuroimaging research has redefined broad categories of functional division in the human brain. Specifically, it has shown that (i) primary processing, (ii) task-positive nonprimary processing, and (iii) task-negative (default-mode) processing are three central poles of neural macroscale functional organization (Greicius et al. 2003; Fox et al. 2005; Margulies et al. 2016). Primary processing includes motor, somatosensory, auditory, and visual systems. Nonprimary task-positive processing includes top-down goal-directed systems active in attention demanding activities such as working memory tasks, and bottom-up stimulus-driven systems that direct attention toward salient stimuli (Corbetta and Shulman 2002; Fox et al. 2006; Seeley et al. 2007). Task-negative regions are engaged in abstract higher-order association processes, which are furthest removed from primary systems (Mesulam 1998; Margulies et al. 2016) and anticorrelated with task-positive networks (Fox et al. 2005; Zhou et al. 2018), including unfocused processes with low attentional demands

such as mind wandering, and related states of autobiographical memory retrieval and introspection (Greicius et al. 2003; Buckner et al. 2008).

This new macroscale understanding of the range and poles of brain function has revealed that not only the cerebral cortex (Yeo et al. 2011), but also the thalamus (Hwang et al. 2017), striatum (Choi et al. 2012), and cerebellar cortex (Buckner et al. 2011) contribute to a broad spectrum of human neural processing categories. Specifically, primary processing networks such as somatomotor, task-positive networks such as ventral and dorsal attention, and task-negative default-mode network (DMN) are all represented within each of these structures.

Whether the dentate nuclei (DN) of the cerebellum obey a similar set of macroscale functional divisions, and whether the DN are yet another compartment of broad-spectrum representation of human brain function, remains unknown. DN viral tracing studies have described a motor versus nonmotor dichotomy (Dum and Strick 2003), a bi-modal division that has been echoed in human resting-state fMRI (Bernard et al. 2014), task-based fMRI (Küper et al. 2011, 2012, 2014; Thürling et al. 2011), and diffusion tensor imaging (DTI; Steele et al. 2017). Anatomical and neuroimaging investigations indicate that the central components of functional specialization in human DN may extend beyond a dual motor versus nonmotor classification, and span primary, task-positive, and task-negative domains of brain function. First, these systems are all represented in cerebellar cortex (Buckner et al. 2011; Guell et al. 2018b), in close correspondence with cerebral cortical organization (Yeo et al. 2011; Margulies et al. 2016). Second, the DN are a central node in the anatomy of cerebellar connections, relaying the majority of fibers exiting the cerebellar cortex and participating in multiple reverberating systems within the cerebellar circuits.

The DN are the largest and most lateral of the cerebellar nuclei, and receive the majority of cerebellar cortical efferents (Haines and Dietrichs 2012). Ascending projections of the DN are directed principally to the thalamus, connecting cerebellar cortex to thalamo-cortical projections and thus to sensorimotor cortices and higher-order association areas. Multiple reverberating patterns exist in the connectivity between cerebellar cortex, DN, and extracerebellar structures. First, neurons in DN project back to cerebellar cortical areas from which they receive input (Dietrichs 1981). Second, each inferior olivary nucleus (i) projects directly to a specific territory of cerebellar cortex, (ii) projects to the DN territory that receives projections from that particular territory of cerebellar cortex, and (iii) at the same time receives projections from that particular DN territory (as reviewed in De Zeeuw et al. 1998). Third, current anatomical evidence points to reciprocal reverberating loops between defined areas of cerebral cortex, pons, cerebellar cortex, dentate, and thalamus. That is, a cerebral cortical area that sends projections to the cerebellar cortex receives feedback from that same cerebellar corticonuclear microcomplex (Kelly and Strick 2003). This rich set of connections provides an anatomical basis for the hypothesis that a broad range of macroscale functional categories in the brain are represented in DN.

Gradient-based and data-driven clustering analyses of resting-state data, a methodology that remains largely unexplored in DN, can provide critical information necessary to test this hypothesis. The identification of the main functional subdivisions of human DN requires a data-driven approach independent from a priori assumptions regarding the nature and localization of functional domains, and flexible to include as many components as necessary to fully identify the principal poles and spectrum of DN specialization.

Here, we set out to identify for the first time the central components of functional organization in human DN. We used gradient-based and data-driven clustering methods that have previously unmasked these central aspects of functional neuroanatomy in cerebral (Margulies et al. 2016) and cerebellar cortex (Guell et al. 2018b). Sixty-four-channel resting-state MRI data combined with simultaneous multislice (SMS) acquisition provided unprecedented DN spatial and temporal resolution useful to overcome technical difficulties of functional mapping in small brain territories. We then attempted to replicate our results in a separate set of participants, validating our findings and their utility for future independent human studies of DN.

## Materials and Methods

### Study Participants

Sixty right-handed participants were included in this study, of which 20 participants (10 male, mean age = 13.64, age range = 12–14) were included in the discovery sample, and 40 participants (18 male, mean age = 15.13, age rage = 14–16) were included in the replication sample (a supplementary analysis in an adult sample is described later in this section). These participants were recruited as control subjects as part of two ongoing larger studies (one study examined brain correlates of depression and anxiety in adolescents, and another study investigated brain correlates of cognitive processing, social processing, socioeconomic status, and academic achievement in adolescents). Written informed parental consent, and assent from participants, was collected from all subjects in accordance with guidelines established by the Massachusetts Institute of Technology Committee on the Use of Humans as Experimental Subjects (discovery sample) and the Partners Health Care Institutional Review Board (replication sample). None of the participants had a self-reported or family-reported history of psychiatric or neurological illness.

### MRI Structural and Resting-State Data

Imaging data for the discovery and replication samples were collected on two distinct 3 T Siemens PRISMA MRI scanners with vendor-provided 64 Channel (64Ch) head coil (Siemens Healthcare). Both scanners corresponded to the same model and all participants within each sample were scanned in the same scanner. Scanning parameters were identical for both the discovery and replication samples. High-resolution structural data (0.8 mm isotropic voxels) were acquired using a T1-weighted MPRAGE sequence with duration 7 min 50 s (in-plane acceleration factor of 2). Scan parameters for TR/TE/TI/Flip Angle were 2.4 s/2.18 ms/1.04 s/8°. Anatomical scans were immediately followed by resting-state scans, during which subjects were asked to stay awake and keep their eyes fixated on a cross hair. Two resting-state sessions per participant were acquired for the discovery sample, and four sessions per participant were acquired for the replication sample. Scan parameters (T2*-weighted EPI sequence) for TR/TE/Flip Angle/echo spacing/bandwidth were 800 ms/37 ms/85°/0.58 ms/2290 Hz-per-pixel. Seventy-two interleaved (ascending/foot-head) slices were collected in AC-PC plane using an autoalign procedure to minimize intersubject variability in data acquisition. Participants

wore noise-canceling devices during structural and resting-state scanning (passive noise canceling disposable earplugs (3 M 1100) in replication sample, and active Sensimetrics S14 noise canceling earphones in discovery sample). The combination of 64Ch array coil and SMS acquisition (multiband factor of 8) (Setsompop et al. 2012) provided high temporal sampling (420 time points during an acquisition window of 5 min and 46 s for each session in the discovery and replication samples) and high spatial resolution (2 mm isotropic), while maintaining whole-brain coverage (including the entire cerebellum). Of note, 64Ch array coils tolerate relatively high multiband factors (8 in the present study) providing improved signal-to-noise ratio (SNR) for all brain areas as demonstrated previously (Keil et al. 2013). Further, unlike in-plane acceleration, SMS imaging strategies to increase temporal sampling have no SNR penalty for multiband acceleration (Setsompop et al. 2012).

### Data Analysis: Preprocessing and Calculation of Connectivity Matrix From Dentate Nuclei to Cerebral Cortex

EPI data were realigned, normalized to MNI template, and spatially smoothed with a 4-mm FWHM Gaussian kernel using SPM12 (Wellcome Department of Imaging Neuroscience; www.fil.ion.ucl.ac.uk/spm). Structural images were segmented into white matter, gray matter, and cerebrospinal fluid using SPM12 (Ashburner and Friston 2005). CONN Toolbox (Whitfield-Gabrieli and Nieto-Castanon 2012) was used for calculating connectivity from DN to the whole brain, but only connectivity data from DN to cerebral cortex were used in our analyses. Conn, with over 75 000 downloads, is an in-house developed software tool that covers the entire pipeline from raw fMRI data to hypothesis testing. The toolbox integrates multiple state-of-the-art resting-state preprocessing and analysis algorithms, including tools that are developed specifically for removing physiological noise (such as anatomical component-based correction method (aCompCor, Behzadi et al. 2007)) and comprehensive quality assurance methods. In this way, Conn facilitates the implementation of integrated analysis pipelines that are developed by experts in the field of resting-state fMRI data analysis. In the discovery sample, for each voxel within DN (as defined using the SUIT DN mask; Diedrichsen et al. 2011), a 2-mm sphere seed was generated and used as a region of interest for seed-to-voxel whole-brain analysis. Band-pass filtering was executed at 0.008–0.09 Hz (which corresponds to default band-pass filtering values in Conn). The Artifact Detection Toolbox (http://www.nitrc.org/projects/artifact_detect) was used for denoising, as follows. Time points with mean signal intensity outside three standard deviations from global mean, and 0.5 mm scan-to-scan motion were flagged as invalid scans and were regressed out along with the six realignment parameters and physiological sources of noise (i.e., three principal components of white matter, and three principal components of cerebrospinal fluid segments, using aCompCor; Behzadi et al. 2007). Whole brain correlation maps derived from denoised time-series from each voxel in DN for each participant in the discovery sample were used for functional gradient calculations, as follows.

### Data Analysis: Calculation of Functional Gradients

Based on novel analytical strategies introduced by Coifman et al. (2005), functional gradient analyses of resting-state data have unmasked the principal poles and components of functional neuroanatomy in previous investigations of cerebral cortex (Margulies et al. 2016) and cerebellar cortex (Guell et al. 2018b). Here, we applied this technique for the first time to the study of resting-state data in DN. In brief, this methodology analyses the similarity between the connectivity patterns of each datapoint within a given brain structure, and extracts functional gradients that represent the principal poles and transitions of connectivity patterns within that structure. More specifically, our analysis started by constructing a connectivity matrix including resting-state correlation values from each voxel in DN to each voxel in cerebral cortex (as described in the previous section). The connectivity pattern of each DN voxel was thus represented as an $n$-dimensional vector, where $n$ corresponded to the total number of voxels in the cerebral cortex. Because all DN voxels were represented in the same $n$-dimensional space, cosine distance between each pair of vectors could be calculated, and an affinity matrix was constructed as (1 – cosine distance) for each pair of vectors. This affinity matrix represented the similarity of connectivity patterns for each pair of DN voxels. A Markov chain was then constructed using information from the affinity matrix; information from the affinity matrix was thus used to represent the probability of transition between each pair of vectors. In this way, there was higher transition probability between pairs of DN voxels with similar connectivity patterns. This probability of transition between each pair of DN voxels was analyzed as a symmetric transformation matrix, allowing the calculation of eigenvectors. Eigenvectors derived from this transformation matrix represented the principal orthogonal directions of transition between all pairs of voxels in DN. Diffusion map embedding using functional connectivity values from DN to cerebral cortex thus captured the principal functional gradients of DN functional neuroanatomy. See https://github.com/satra/mapalign for an implementation of this methodology, and our online repository for the application of this methodology to our data (https://github.com/xaviergp/dentate).

### Data Analysis: Clustering of Functional Gradients

Functional gradient values are a continuous measure useful for establishing groups (clusters) of DN voxels based on functional similarity. As functional gradients capture relevant dimensions of DN functional neuroanatomy, groups of voxels in DN can be clustered together based on the similarity of their functional gradient values. In this way, the optimal number of functional divisions of DN, and the location of these principal poles and components of DN functional neuroanatomy, can be identified.

We used data-driven methods to establish clustering analysis parameters, including the number of functional gradients to include in the clustering analysis, and the number of clusters that the clustering analysis should detect, as follows. First, eigenvalues of each functional gradient were used to establish the data variability explained by each component, and thus to establish the set of functional gradients (g) that should be included in the clustering analysis. Only those functional gradients explaining a relevant portion of data variability (as determined when visualizing the curve of percentage variability explained by each functional gradient) were considered to represent a relevant aspect of DN functional neuroanatomy, and thus included as dimensions for the clustering analysis. Then, silhouette coefficient analysis was used to identify the optimal number of clusters (c) to be computed for that set of functional gradients (g) (Hastie et al. 2009). Using scikit-learn (Pedregosa and Varoquaux 2011), $k$-means separated DN voxels in $c$ clusters,

minimizing the sum of the squared differences of each data point from the mean within each cluster in a $g$-dimensional functional space.

Because clustering took place in functional rather than anatomical space, clusters identified were not necessarily composed of contiguous voxels in DN anatomical space. To reduce noise in the spatial distribution of our final DN parcellation, an anatomical cluster-size threshold was used, so that only anatomical clusters containing 10 or more contiguous voxels were included in our final definition of functional territories in DN.

DN–cerebral cortical connectivity data used to define the borders of DN functional territories were smoothed in cerebral cortex but not in DN or any of its neighboring structures. An advantage of this approach is that it minimized partial volume effects from structures close to DN such as white matter, cerebellar cortex, fastigial, and interposed nuclei, while allowing optimization of SNR in cerebral cortical data.

### Data Analysis: Post hoc Characterization of Connectivity From DN Clusters and Validation

To characterize the functional significance of each identified functional territory in DN, each DN functional territory was used as a seed in a seed-to-voxel resting-state functional connectivity analysis. Using the CONN Toolbox (Whitfield-Gabrieli and Nieto-Castanon 2012), Pearson's correlation coefficients were computed using the denoised time courses, and then converted to normally distributed z-scores using Fisher transformation to allow second-level general linear model analyses. To test the possibility that each cluster in DN represented a functional domain that was different from the functional domain of other clusters (unique effect), seed-to-voxel analyses were also calculated by computing the effect of each functional territory against the effect of all other functional territories. The same analyses were performed in the independent replication dataset. Functional connectivity from each functional territory was first visualized after thresholding at the 95th percentile of $r$ median correlation values in the discovery sample—namely, using the same thresholding and sample that was used when calculating functional gradients. We then performed unique effect analyses that were based on statistical significance thresholding, including $p < 0.001$ at the voxel level with a $p < 0.05$ FDR cluster-size correction, in both the discovery and replication samples. An additional lower threshold was also used in the replication sample ($p < 0.005$ at the voxel level with a $p < 0.05$ FDR cluster-size correction) to allow better visualization of brain networks in our results. Our characterization of DN functional neuroanatomy was based on functional connectivity to cerebral cortex; in addition, as a supplementary analysis, we surveyed functional connectivity maps in cerebellar cortex and thalamus from each functional territory identified in DN. Seed-to-voxel analyses to characterize connectivity to cerebral cortex from each identified functional territory in DN were also calculated without smoothing; this supplementary analysis was performed to minimize partial volume effects from structures close to DN.

### Data Analysis: Validation in an Adult Sample

The analyses described thus far used data that were acquired in adolescents using 64Ch array coils and SMS. These adolescent 64Ch SMS data provided high temporal and spatial resolution, but raised the question of whether our characterization of DN functional architecture would remain observable in an adult population. Studies in adolescents indicate that basic network organization—what the principal brain functional networks are (DMN, attentional, and primary), and their position in the brain—does not change from adolescence to adulthood (see first figure in Marek et al. 2015, comparing network organization in childhood, early adolescence, late adolescence, and adulthood). To test this prediction, we added an adult sample to our set of replication analyses. As these data were not obtained using 64Ch array coils but instead used a more conventional 32Ch array, this analysis also provided the opportunity to examine if the same functional territories in DN would remain observable in studies not using 64Ch data. Data for this analysis were downloaded from the Autism Brain Imaging Data Exchange (ABIDE) dataset (Di Martino et al. 2014), including a total of 17 healthy control participants (12 male, mean age = 21.94, age range = 19–26) that were all scanned at Indiana University (IU) using a Siemens Magnetom TrioTim 3 T MRI scanner. T1-weighted MPRAGE sequence had a duration of 7 min 2 s (in-plane acceleration factor of 2), TR/TE/TI/Flip Angle of 2400 ms/2.3 ms/1000 ms/8°, and spatial resolution of 0.7 mm isotropic voxels. Resting-state scan parameters (T2*-weighted EPI sequence) for TR/TE/Flip Angle/echo spacing/bandwidth were 813 ms/28 ms/60°/0.49 ms/2604 Hz-per-voxel, 42 slices, with a duration of 16 min 21 s (1200 time-points, out of which the initial 433 images (~6 min) of the entire acquisition were publicly available), and spatial resolution of 3.4 mm isotropic voxels. The dataset from IU was selected given that it provided the most similar TR values and number of time points when compared with our adolescent discovery and replication samples (0.813 s and 433 in IU, versus 0.8 s and 420 in our adolescent discovery and replication samples). Informed consent was obtained at that institution. Functional connectivity from each identified functional territory was calculated using the same seed-based analysis steps and parameters as in the adolescent discovery and replication samples, as described in the previous sections.

### Data Analysis: Visualization of Dentate–Cerebral Cortical Functional Connectivity Weighted as a Factor of Dentate Functional Gradients

An alternative visualization of the significance of DN functional gradients was performed in the discovery sample using a method independent of clustering analyses. In this approach, functional connectivity from dentate to cerebral cortex was weighted as a factor of DN functional gradient values. These weighted functional connectivity maps of DN—cerebral cortical functional connectivity were calculated as follows. For each DN functional gradient (G) and each DN voxel (V), the cerebral cortical functional connectivity map of each voxel V was multiplied by the G value of V. For example, for DN functional gradient 1, cerebral cortical functional connectivity map of voxel A was multiplied by the functional gradient 1 value of voxel A; cerebral cortical functional connectivity map of voxel B was multiplied by the functional gradient 1 value of voxel B; and so on for each voxel in DN. Then, all weighted cerebral cortical functional connectivity maps (as many as the total number of voxels in DN) were added together. The resulting cerebral cortical maps (one for each DN functional gradient) provided a visualization of the significance of each DN functional gradient in terms of functional connectivity to cerebral cortex that was independent from clustering analyses. These maps were compared with intracerebral cortical functional gradients as reported by (Margulies et al.

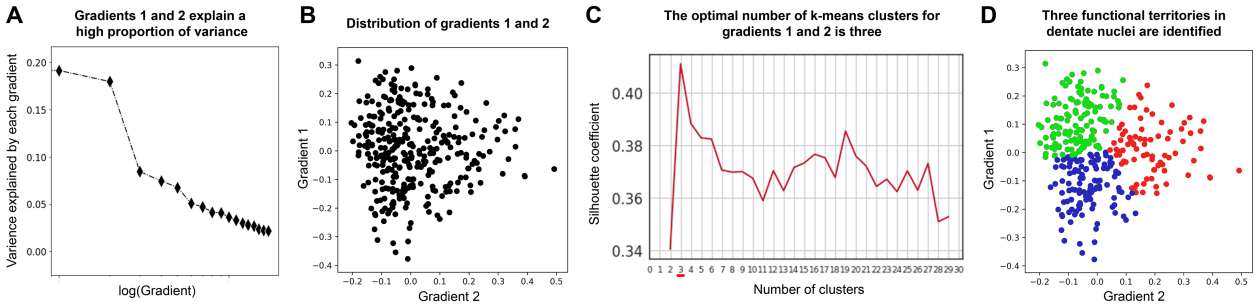


Figure 1. Data-driven identification of the number and location of functional territories in DN. (*A*) Functional gradients 1 and 2 capture the majority of variability in DN resting-state functional connectivity to cerebral cortex. Note a clear knee in the curve of variability explained by each functional gradient, indicating that the first two components are the most relevant aspects of DN functional neuroanatomy. (*B*) Distribution of DN functional gradients 1 and 2. Each dot in this graph corresponds to one voxel in left or right DN. (*C*) Silhouette coefficient analysis identified three as the optimal number of *k*-means clusters when grouping DN voxels according to their functional gradient 1 and 2 values. Note that the maximum score is achieved with three clusters. (*D*) K-means clustering grouped DN voxels in three categories according to their functional gradient 1 and 2 values. Each functional territory is shown here in a different color (red, blue, and green), and these three colors correspond to the three functional territories shown in Figure 2A and 2B. See our online repository to access all custom code used for these analyses, https://github.com/xaviergp/dentate.

2016). Maps by Margulies and colleagues were reproduced using their publicly available code and the same public data used in their investigation (for details see Margulies et al. 2016).

## Results

### Overview

Functional gradients 1 and 2 captured the highest portion of variability in DN resting-state functional connectivity to cerebral cortex (Fig. 1A). Silhouette coefficient analysis identified three as the optimal number of *k*-means clusters when grouping DN voxels according to their functional gradient 1 and 2 values (Fig. 1C). These three territories in DN corresponded uniquely to (i) DMN; located rostral-ventrally in right and left DN, and also caudally in right DN; (ii) salience-motor network; located centrally in the rostral-caudal axis in right and left DN; and (iii) visual network; located caudally in left DN, and central-caudally in right DN (cluster locations within DN are shown in Figure 2A; functional connectivity patterns in cerebral cortex from each DN cluster are shown in Figure 2B). These functional connectivity patterns were successfully replicated in an independent dataset of adolescents (Fig. 2B) and adults (see **Supplementary Fig. 1**), and further confirmed using an alternative visualization independent of clustering analyses (Fig. 3).

Note that the DN functional territories were identified in the discovery sample using gradient-based analyses followed by clustering-based analyses (Fig. 1). Seed-based functional connectivity from each territory was analyzed first in the discovery sample and then replicated in the independent datasets. In this way, replication analyses of functional connectivity patterns were performed in datasets that did not influence the spatial distribution of functional territories in the DN.

### Identification of the Most Relevant Functional Gradients of Dentate Nuclei

The first step to define the number and nature of functional territories in DN was to determine the amount of variance explained by each functional gradient. We observed a clear knee in the curve of data variability explained by each functional gradient, indicating that functional gradients 1 and 2 were the most relevant components of DN connectivity to cerebral cortex (Fig. 1A; gradient 1 explained variability = 19.14%, gradient 2 = 17.95%, gradient 3 = 8.43%, and gradient 4 = 7.45%). For this reason, only functional gradients 1 and 2 were included in further analyses. Clustering of voxels in DN based on functional gradients 1 and 2 values, and calculation of functional connectivity from each resulting cluster in our discovery and replication samples, provided a successful data-driven identification and characterization of DN functional territories, as follows.

### Identification of the Optimal Number of Functional Territories in Dentate Nuclei

As functional gradients 1 and 2 captured the highest portion of DN resting-state variability in our data, we considered that functional gradients 1 and 2 were an optimal dimensional space for the identification of functionally distinct territories in DN. A remaining question was the number of functional territories that our clustering analysis ought to identify. Unlike previous investigations that assumed a bi-modal motor versus nonmotor division, we did not impose a priori assumptions to determine the number of functional divisions with the DN. Instead, we conducted silhouette coefficient analysis and in this way determined that three was the optimal number of *k*-means clusters when grouping DN voxels according to their functional gradient 1 and 2 values (Fig. 1D). We therefore concluded that three is the optimal number of functional subdivisions in human DN as indexed by high spatio-temporal resolution resting-state MRI in our sample.

### Clustering of Three Functional Territories in the Dentate Nuclei

*K*-means calculation of three clusters was performed based on functional gradient 1 and 2 values (Fig. 1D). This analysis required that all DN voxels contained within each functional territory were contiguous in functional gradients 1 and 2 coordinates (as shown in Fig. 1D), but not necessarily contiguous in spatial coordinates. When grouped according to spatial localization in DN, multiple subclusters were identified for each of the three functional territories. Size and localization of each subcluster is reported in **Supplementary Table 1**. A minimum size of 10 contiguous voxels in spatial coordinates was

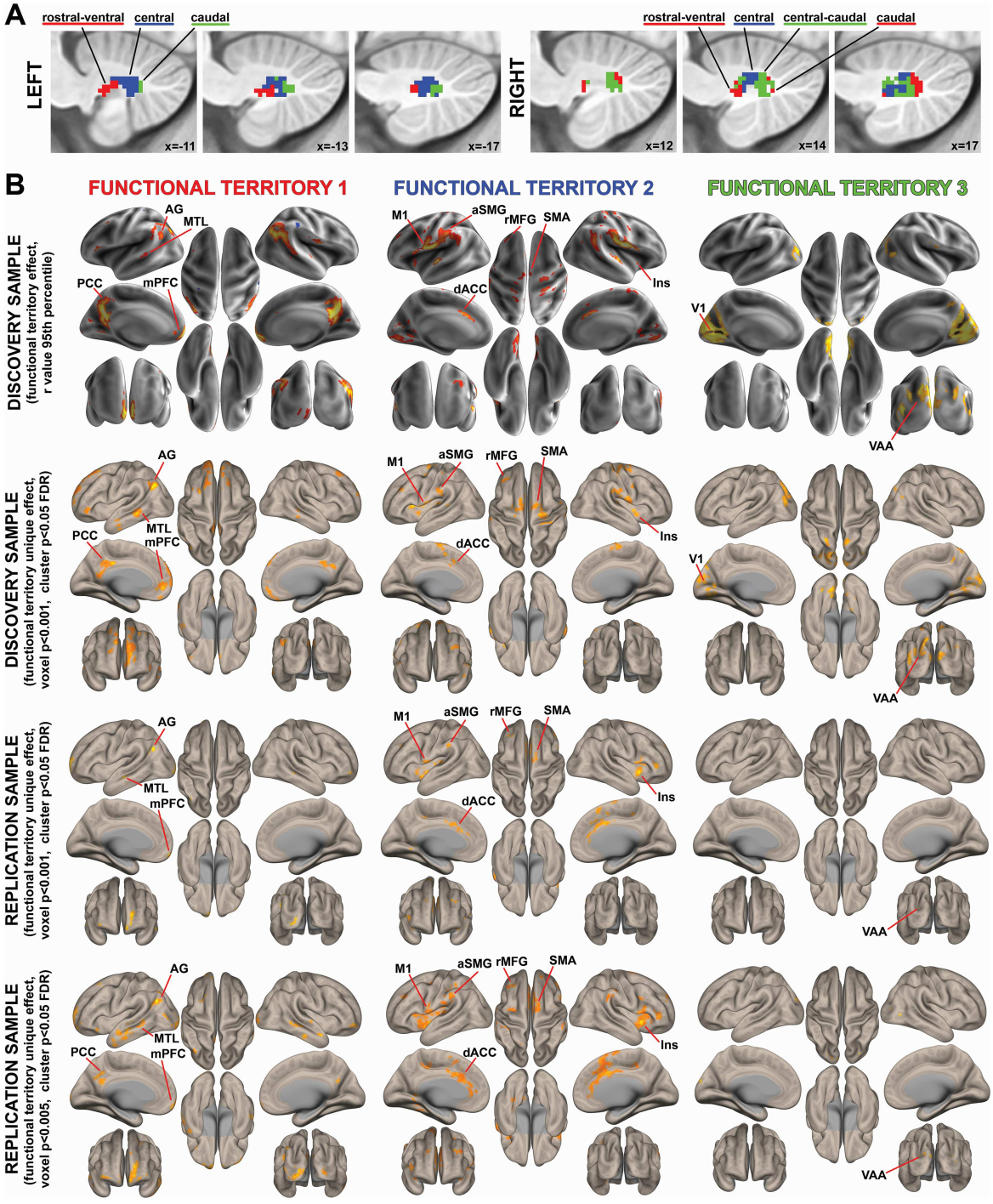


Figure 2. Spatial location and functional characterization of functional territories in DN. Green, red, and blue colors correspond to the same territories in Figures 1D, 2A, and 2B. (A) Spatial location of the three functional territories identified as shown in Figure 1D. (B) Each functional territory identified in DN exhibited a unique functional connectivity pattern to cerebral cortex that corresponded to well-established brain networks. Specifically, functional territories 1, 2, and 3 corresponded to default-mode, salience-motor, and visual networks, respectively. First row: 95th percentile of median $r$ values in the discovery cohort. Second row: statistical significance thresholding of the unique effect of each functional territory (e.g., functional territory 1 > functional territories 2 and 3), voxel $p < 0.001$ with cluster size FDR correction of $p < 0.05$. Note that calculations of unique effects are relevant as they provide statistical proof for the conclusion that functional connectivity from each functional territory in DN is different from the rest of territories. Third row: statistical significance thresholding equal to second row, but in an independent replication sample. Note that a replication analysis is important as it provides reassurance that functional territories reported here are not overfitted to the discovery sample. Fourth row: same analysis as third row, but with lower statistical thresholding to allow better visualization of brain networks (voxel $p < 0.005$ with cluster size FDR correction of $p < 0.05$). AG, angular gyrus; MTL, medial temporal lobe; PCC, posterior cingulate cortex; mPFC, medial prefrontal cortex; aSMG, anterior supramarginal gyrus; M1, primary motor cortex; rMFG, rostral middle frontal gyrus; SMA, supplementary motor area; Ins, insula; dACC, dorsal anterior cingulate cortex; V1, primary visual cortex; and VAA, visual association area.

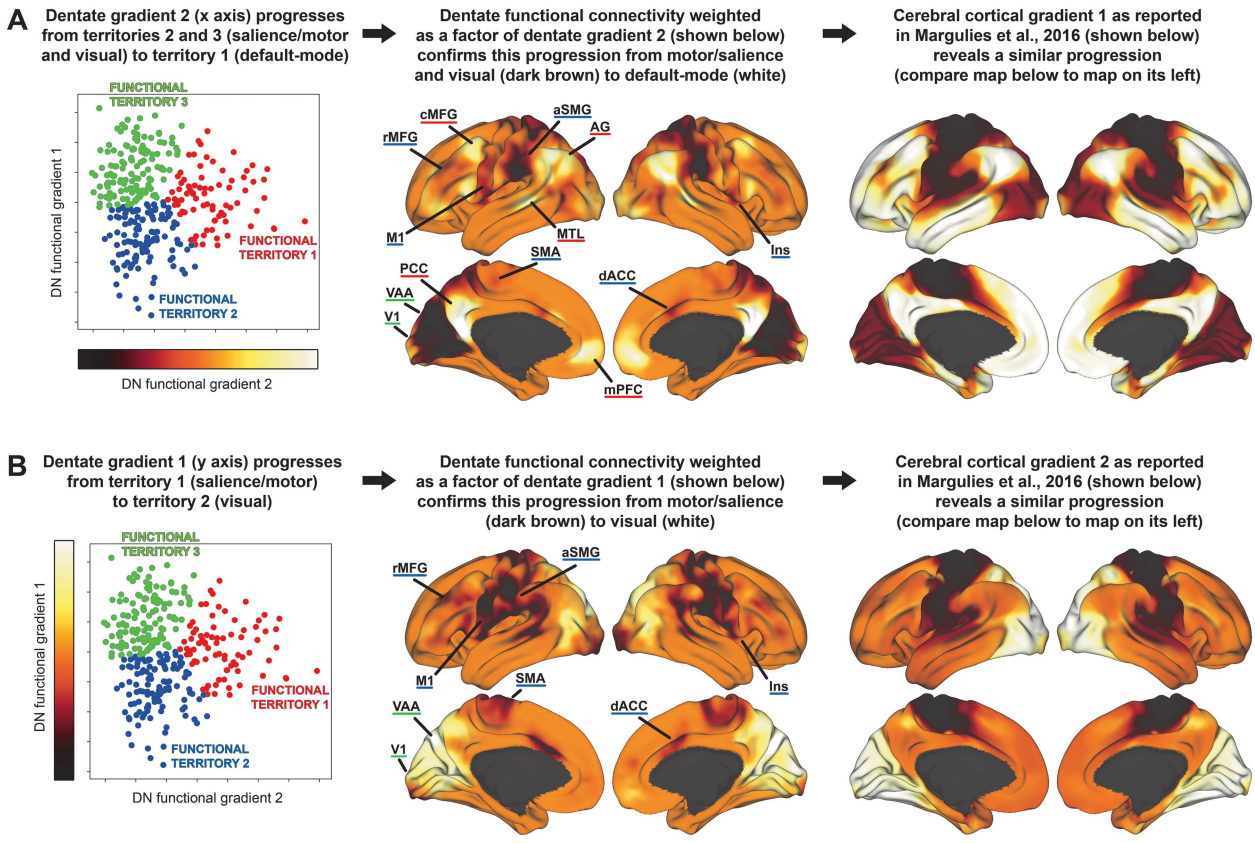


Figure 3. Dentate–cerebral cortical functional connectivity weighted as a factor of dentate functional gradients. (*A*) Dentate functional gradient 2 captures a progression from functional territories 2 and 3 (as characterized in Figure 2*B*, with connectivity to Ins, dACC, aSMG, rMFG, M1, SMA, V1, and VAA) to functional territory 1 (PCC, mPFC, AG, MTL, and cMFG). (*B*) Dentate functional gradient 1 captures a progression from functional territory 2 (Ins, dACC, aSMG, rMFG, M1, and SMA) to functional territory 3 (V1, VAA). Right column: the distribution of dentate functional gradients 1 and 2 visualized in this way is similar to the distribution of the two principal gradients of intracerebral cortical functional connectivity as reported by (Margulies et al. 2016). Abbreviations are the same as in Figure 2; note that cMFG refers to caudal MFG.

imposed in order to eliminate noise in the spatial distribution of each functional territory. This resulted in the retention of three clusters for functional territory 1 (one in left DN located rostral-ventrally, one in right DN located rostral-ventrally, and one in right DN located caudally), two clusters for functional territory 2 (one in left DN and one in right DN, both located centrally along the rostral-caudal axis), and two clusters for functional territory 3 (one in left DN located caudally, and one in right DN extending from central to caudal territories along the rostral-caudal axis) (Fig. 2*A*). DN masks included 339 voxels. Each voxel was 2 mm isotropic (8 $mm^3$), making a total DN volume of 2712 $mm^3$. The size of functional territories 1, 2, and 3 was 936, 936, and 512 $mm^3$, respectively (total DN volume percentage of 34.51%, 34.51%, and 18.88%, respectively). Before excluding voxels that did not belong to clusters of 10 or more contiguous voxels, these volumes were 1056, 1024, and 632 $mm^3$, respectively, corresponding to total DN volume percentages of 38.94%, 37.76%, and 23.3%. The exclusion of voxels that did not belong to clusters of 10 or more contiguous voxels resulted in the retention of 88.64%, 91.41%, and 81.01% of total volume from the uncorrected functional territories 1, 2, and 3, respectively (see **Supplementary Table 1** for further details). Results of both thresholded (minimum size 10 voxels) and unthresholded functional territories are included in our online repository, but only thresholded maps are shown here.

## Characterization of Functional Territories in Dentate Nuclei

Having identified the optimal number and spatial location of functional territories in DN, we aimed to characterize the functional contribution of each territory. This characterization was based on seed-to-voxel resting-state function connectivity analyses from each DN functional territory to cerebral cortex. This approach revealed three distinct functional connectivity patterns (Fig. 2*B*), as follows: The first territory was functionally connected to the DMN, including connectivity to medial prefrontal cortex (mPFC), posterior cingulate cortex (PCC), angular gyrus (AG), and middle temporal lobe (MTL). The second territory corresponded to a salience-motor network, including connectivity to primary motor cortex (M1) and supplementary motor area (SMA), as well as insula (Ins), dorsal anterior cingulate cortex (dACC), anterior supramarginal gyrus (aSMG), and rostral middle frontal gyrus (rMFG). The third territory corresponded to a visual network, including connectivity to primary visual (V1) and visual association areas (VAA). These networks were observable when visualizing functional connectivity maps based on median 95th percentile-thresholded *r* values in the discovery sample—namely, the same thresholds and sample that were used when calculating functional gradients (Fig. 2*B*, first row). These networks were also observable when performing statistical

significance thresholding (voxel and cluster-based $p$ value thresholds) and calculating unique effects of connectivity from each DN functional territory (i.e., functional territory 1 > functional territory 2 + 3; functional territory 2 > functional territory 1 + 3; and functional territory 3 > functional territory 1 + 2) in the discovery sample (Fig. 2B, second row). This analysis of unique effects is relevant, as it provides statistical proof for the conclusion that connectivity patterns from each DN functional territory are different from the connectivity patterns of the other two DN functional territories in our sample. This conclusion would not be fully supported if connectivity effects from each functional territory were only analyzed independently. Importantly, similar patterns of connectivity were replicated in an independent sample in adolescents (shown in two different statistical thresholds in Fig. 2B, third and fourth rows) and adults (shown using the same statistical thresholds in **Supplementary Fig. 1**). These replication analyses are relevant as they support the use of these DN regions in future independent human studies of DN (including adult human samples), providing reassurance that DN functional territories described here are not overfitted to one particular sample. Excluding overfitting is especially relevant given that the structure of our functional gradients and clustering methodology is designed to identify territories in DN that show distinct functional connectivity patterns with cerebral cortex. The same patterns of connectivity were observed when using unsmoothed data (see **Supplementary Fig. 2**).

### Validation in an Adult Sample

Connectivity patterns from each functional territory in DN in the adult sample replicated the networks observed in our main analyses (see **Supplementary Fig. 1**; compare with Fig. 2B). As in the adolescent population, functional territory 1 in the adult cohort engaged PCC and AG (DMN), as well as left caudal MFG which is also part of DMN (see left middle frontal gyrus in Yeo et al. 2011). Functional territory 2 engaged Insula, dACC, rostral MFG, and SMA (motor/salience network). Note the clear dissociation between a DMN contribution in caudal MFG contrasting with a salience/ventral attention network contribution in rostral MFG (as in Yeo et al. 2011). Functional territory 3 engaged VAA (visual network).

### Dentate–Cerebral Cortical Functional Connectivity Weighted as a Factor of Dentate Functional Gradients

As expected from the results of clustering analysis (Figs 1D and 2B), a visualization of cerebral cortical functional connectivity from DN weighted as a factor of each functional gradient confirmed that DN functional gradient 1 captured a progression from functional territory 2 (as characterized in Fig. 2B; connectivity to Ins, dACC, aSMG, rMFG, M1, and SMA) to functional territory 3 (connectivity to V1, VAA) (Fig. 3B). DN functional gradient 2 captured a progression from functional territories 2 and 3 (connectivity to Ins, dACC, aSMG, rMFG, M1, SMA, V1, and VAA) to functional territory 1 (connectivity to PCC, mPFC, AG, MTL, and cMFG) (Fig. 3A). Of note, the distribution of dentate functional gradients 1 and 2 visualized in this way was similar to the distribution of the two principal gradients of intracerebral cortical functional connectivity as reported by Margulies et al. (2016). While Margulies and colleagues defined the three principal poles of cerebral cortical functional neuroanatomy as default-mode, primary motor/auditory, and primary visual areas, note that VAAs are also observed together with primary visual areas in their figures, and salience processing territories such as Ins, dACC, and rMFG are also observed together with primary motor areas in their figures (see Fig. 3, right column; or see figures in Margulies et al. 2016).

### Exploratory Analyses in Cerebellar Cortex and Thalamus

Functional connectivity maps shown in Figure 2B and **Supplementary Figure 1** were visualized in cerebellar cortex and thalamus. For thalamus, functional territories 1 and 3 did not survive our statistical thresholds in any cohort (discovery or replication samples). This observation is likely related to the fact that fMRI signal in cerebral cortex is superior in terms of SNR (given the brain's location in relationship to MRI receiving coils). Functional territory 2 revealed connectivity to some thalamic regions, but the identified maps in the discovery cohort did not overlap with any map in the replication cohorts (adolescent or adult), making these results unreliable. Similarly, for the cerebellar cortex, maps in the discovery cohort for functional territories 1, 2, and 3 did not overlap with maps in the replication cohorts (adolescent or adult), also making cerebellar cortical findings unreliable. Only cerebral cortical results are reported in the present investigation because they were observable in both the discovery and replication samples.

## Discussion

Here, we show for the first time that human DN are optimally divided into three functional territories as indexed by high spatio-temporal resolution resting-state MRI of 60 healthy participants, and that these three territories contribute uniquely to default-mode, salience-motor, and visual brain networks. Contrasting with previous views that define motor versus nonmotor territories as the principal poles of DN organization, the results presented here indicate that DN subdivisions span a broad range of human macroscale neural specialization categories, namely, default-mode, attentional-motor, and visual. These conclusions are supported by the analytical strategies of 64-channel MRI imaging, data-driven methodology, and replication in an independent sample.

### Human Dentate Nuclei are Divided into Default-Mode, Salience-Motor, and Visual Processing Territories, Echoing a Broad Spectrum of Human Macroscale Neural Specialization

Each functional territory identified within the DN exhibited a unique pattern of functional connectivity with the cerebral cortex that corresponded to well-established brain networks (Fig. 2). Here, we argue that a broad spectrum of human macroscale neural specialization is represented in DN, and that central components of this spectrum of functional diversity are segregated in distinct functional territories within DN.

Functional territory 1 corresponded to DMN, which we conceptualize here as the apex of the central axis of human macroscale brain organization, as follows. Functions in the human brain can be classified according to multiple criteria. One fundamental classification method distinguishes sequential hierarchical levels of information processing—from primary processing cortices, to intramodality association areas, and progressively transmodal processing in heteromodal, paralimbic,

and limbic cortices. This unimodal-to-transmodal progression is subserved by cerebral short association fibers that link primary processing cortices to progressively higher transmodal brain territories (Pandya and Yeterian 1985; Mesulam 1998). This fundamental axis of human brain organization can be captured in vivo in cerebral cortex (Margulies et al. 2016), and it has been recently shown that cerebral-cerebellar anatomical connectivity results in a remarkably similar organization in cerebellar cortex (Guell et al. 2018b). Along this central unimodal-to-transmodal axis of brain specialization, DMN is situated at the highest transmodal extreme (Margulies et al. 2016; Guell et al. 2018b), with functional contributions revolving around unfocused cognitive processing such as mind wandering and related mental states of autobiographical memory retrieval and introspection (Buckner et al. 2008). The DMN is also involved in active introspectively-oriented processes such as accessing memory about other people's thoughts in false beliefs tasks (Cabeza et al. 2012). Within this context, there is a large and expanding body of literature linking cerebral and cerebellar DMN to social cognition (Buckner et al. 2008; Van Overwalle 2009; Van Overwalle and Baetens 2009; Schurz et al. 2014; Van Overwalle et al. 2014, 2015, 2019). All central nodes of DMN were included in cerebral cortical connectivity from functional territory 1, namely, PCC, mPFC, AG, and MTL (Buckner et al. 2008).

Functional territory 2 corresponded to salience-motor network, presented here as the cognitive opposite pole of DMN. Specifically, attentional functions in the brain are fundamentally distinct and arguably opposite to default-mode cognitive processes such as mind wandering and internally-oriented thought. This view is supported across multiple human and animal studies of brain physiology. Attentional and DMN territories are anticorrelated at rest (Fox et al. 2005), dissociated in vigilant as opposed to inattentive brain state activity (Hayden et al. 2009; Barch et al. 2013), and causally interfere with the activation of each other (Chen et al. 2013). Within the realm of attention, cognitive neuroscience clearly delineates a fundamental distinction between goal-directed and stimulus-driven processes. Attention directed by top-down cognition is in clear contrast with attention dominated by external events (Corbetta and Shulman 2002). This distinction is also echoed in the intrinsic organization of brain functional architecture (Fox et al. 2006; Seeley et al. 2007)—such investigations have resulted in the definition of multiple attentional brain networks such as dorsal attention network and salience network. While all attentional systems are dissociated from DMN, salience network is uniquely segregated from DMN function because it is responsible for the sharp transition from inattentive/default-mode states to vigilant states (Sridharan et al. 2008; Goulden et al. 2014; Zhou et al. 2018). Thus in contrast with functional territory 1, functional territory 2 revealed functional connectivity to all central nodes of salience network, namely, insula and dACC (Seeley et al. 2007), as well as secondary salience-linked territories including rMFG and aSMG (see their connectivity to insula and dACC in Yeo et al. 2011, 17-network parcellation).

Functional territory 2 also revealed connectivity to motor territories M1 and SMA, which we view here as a characterization of the nature of attentional processing in DN. It is well established that stimulus-driven attentional control is linked to sensorimotor systems, with anatomical studies revealing sensorimotor afferent and efferent projections in insula (Mesulam and Mufson 1982; Mufson and Mesulam 1982), and neuroimaging and invasive stimulation studies in humans confirming a physiological coupling between these two systems (Seeley et al. 2007; Deen et al. 2011; Stephani et al. 2011; Uddin 2015). dACC, included in connectivity from functional territory 2, is involved in salience processing as well as in motor control. It is anatomically linked with salience systems and also with the spinal cord and primary and supplementary motor cortices (Morecraft and van Hoesen 1992; He et al. 1995; see Amiez and Petrides 2014; Loh et al. 2018 for human fMRI evidence). A link between salience and motor processing in DN resonates not only with the well-established role of the cerebellum in motor control, but also with the anatomical and functional connections linking salience processing to sensorimotor processing in the brain.

Functional territory 3 corresponded to the visual network, presented here as the unimodal opposite pole of sensorimotor processing. Clustering of brain territories based on intrinsic functional connectivity patterns identifies somatosensory and visual as the two central unimodal components of brain organization (Yeo et al. 2011), and the transition from sensorimotor to visual functional connectivity patterns is the second largest source of variability in functional gradients of the cerebral cortex (Margulies et al. 2016). Functional territory 3 revealed connectivity to V1 and VAA, defining the third and last central division of human DN organization. Whereas connectivity to V1 was not observed in the replication sample analysis, VAAs were present in both discovery and replication samples, supporting the validity of a visual functional territory in human DN. There does not seem to be a predominant representation of primary visual processing in cerebellar cortex as indexed by fMRI in humans (Buckner et al. 2011). Anatomical tract tracing investigations reveal corticopontine projections from peri- and para-striate cortical regions with a lesser contribution from peripheral field representations in striate cortex in monkey (see Schmahmann and Pandya 1993) and cat (Albus et al. 1981). In contrast, there are large territories of cerebellum devoted to attentional resources relevant for visual association processing (Buckner et al. 2011; Guell et al. 2018b), and cerebro-cerebellar anatomical circuits include cerebral cortical VAA (Fries 1990; Schmahmann and Pandya 1992, 1993). Anatomical projections also connect DN to frontal eye fields (Lynch et al. 1994) and medial and lateral intraparietal areas (Prevosto et al. 2010). There are thus links between the cerebellum and the occipital, frontal, and parietal components of visual attention and spatial cognition in the cerebral cortex. Moreover, recent evidence indicates that visual cognition is not only largely represented in cerebellum, but also organized in retinotopic maps that overlap with top-down attention networks in cerebellar cortex, specifically dorsal attention network (Brissenden and Somers 2019; van Es et al. 2019). Visual association systems in DN may thus correspond predominantly to top-down attentional control, in contrast with salience-motor contributions of functional territory 2 that correspond predominantly to bottom-up attentional control.

### Default-Mode, Salience-Motor, and Visual Processing Domains are Located in Distinct Regions Within the Dentate Nuclei

Our results identified that central components of the spectrum of human neural functional specialization—default-mode, salience-motor, and visual—are segregated in distinct spatial territories within DN (Fig. 2A). Default-mode processing was localized in rostral-ventral aspects of left and right DN, as well as in caudal aspects of right DN. Salience-motor processing was localized centrally along the caudal-rostral axis, and

visual processing was localized caudally. This distribution of salience-motor and visual territories was more apparent in left compared with right DN. Specifically, there was more interdigitation between salience-motor and visual processing territories in right DN than in left DN, and the caudal portions of right DN were occupied both by default-mode and visual processing territories.

The broad functional domain categories identified here (default-mode, salience-motor, and visual) are different from previous descriptions of DN organization centered on a bimodal motor versus nonmotor division. For this reason, the anatomical location of our findings is not directly comparable with previous DN parcellations (Dum and Strick 2003; Bernard et al. 2014; Steele et al. 2017). However, our results align and in some cases contrast with some aspects of previous descriptions of DN functional neuroanatomy, as follows.

Our data-driven approach did not identify any territory of pure primary motor specialization in DN; functional territory 2 revealed functional connectivity to both motor and salience cerebral cortical processing areas. This observation appears to be incompatible with well-established anatomical knowledge that the nonhuman primate dorsal DN is predominantly linked to primary motor cortex (as reviewed in Dum and Strick 2003), and with the extensive evidence supporting a distinction between motor networks and other networks, such as salience, in human fMRI data (e.g., Habas et al. 2009; Yeo et al. 2011). However, a physiological link between motor and salience processing is supported by reports of anatomical and functional connections between these systems (Mesulam and Mufson 1982; Mufson and Mesulam 1982; Seeley et al. 2007; Deen et al. 2011; Stephani et al. 2011; Uddin 2015). Ventral DN territories dedicated to nonmotor control are enlarged in human compared with lower species (Leiner et al. 1991, Matano 2001). Our findings are compatible with this formulation. Human DN territories specialized in pure motor control with connectivity only to sensorimotor territories may be too small, or may represent a too small portion of resting-state data variability, to be identified by our data-driven functional parcellation method as a separate component of human DN functional specialization. The only previous investigation of resting-state human DN functional topography was based on manual resting-state seed location with the specific objective to identify pure motor versus pure nonmotor territories. That study did not successfully identify a DN territory with functional connectivity exclusively to motor systems (Bernard et al. 2014, note that motor seed includes also connectivity to inferior parietal lobule and prefrontal cortex). The evidence presented here is not sufficient to definitively establish whether there is overlap between motor and salience functional territories in human DN, or whether functional patterns as measured by fMRI in these two systems are in fact dissociable. Habas et al. (2009) identified a separate component for motor and salience processing in a whole-brain resting-state fMRI analysis. They reported DN engagement in both components, but the degree of spatial overlap between these two networks in DN was not specifically evaluated. Future human DN studies with higher spatial resolution or improved SNR will be needed to determine whether the motor and salience systems in the DN are indeed separable.

Current consensus in DN functional neuroanatomy is that ventral and caudal territories are specialized in nonmotor control, while dorsal territories are specialized in motor control. This overarching dichotomy was established in anatomical investigations in monkeys (Dum and Strick 2003), and echoed in human investigations of resting-state connectivity (Bernard et al. 2014), task fMRI (Küper et al. 2011, 2012, 2014; Thürling et al. 2011), and tractography (Steele et al. 2017). More fine-grained functional specialization within the DN is exemplified by mapping of nonoverlapping primary motor versus premotor projections within the motor division, and of prefrontal versus posterior parietal projections within the nonmotor division (see Dum and Strick 2003). All three principal subdivisions of DN organization identified in our study contained components of nonmotor control. However, within nonmotor domains, the prediction is that default-mode processing should be located preferentially in ventral territories of DN, as DMN is arguably the apex of a motor-to-nonmotor hierarchy of neural function (Mesulam 1998; Margulies et al. 2016; Guell et al. 2018b). Our findings are consistent with this prediction, as default-mode processing was the only functional territory with a spatial distribution that did not encroach upon dorsal aspects of DN. Specifically, both right and left DN revealed DMN processing that was segregated in rostral-ventral territories. Default-mode processing was also represented in right DN caudal pole. Perhaps consistent with this observation, anatomical connectivity reports map nonmotor processing in the caudal pole of DN in addition to its ventral surface (Dum and Strick 2003), and task fMRI investigations also report nonmotor processing in caudal aspects of DN (Küper et al. 2011, 2014; Thürling et al. 2011).

Representation of DMN in two territories in right DN (rostral-ventral and caudal), contrasting with one territory in left DN (rostral-ventral), is in agreement with whole-brain patterns of DMN lateralization. DMN is more predominantly present in left cerebral cortex (Agcaoglu et al. 2014) and right cerebellar cortex (Buckner et al. 2011). Right DN receives projections from right cerebellar cortex, and right cerebellar cortex is predominantly connected to left cerebral cortex. Stronger representation of DMN in the right DN is consistent with this knowledge. Left cerebral cortical and right cerebellar cortical language processing lateralization might also relate to our observed pattern of stronger lateralization of DMN to right DN. Of note, DMN territories overlap with language processing areas in cerebral and cerebellar cortex as indexed by some task fMRI paradigms (see supplementary material in Guell et al. 2018b) (it is not entirely clear whether this overlap reflects pure language processing in DMN, or rather language-related phenomena such as theory of mind that is often invoked in tasks that include linguistic content). Cerebral cortical maps of connectivity identified here as DMN (Fig. 2, functional territory 1) also included language-related regions such as AG and inferior frontal gyrus (Price 2012), and previous task fMRI experiments have demonstrated stronger language-related processing in right DN compared with left DN (Küper et al. 2011; Thürling et al. 2011). Further, the observation of multiple representations of DMN in right DN raises the larger possibility of network architecture within DN. It has long been established that numerous functional domains are represented in multiple segregated nodes in the cerebral cortex (Selemon and Goldman-Rakic 1988; Cavada and Goldman-Rakic 1989a,b; Yeo et al. 2011). Similarly, there are two representations of motor processing and three representations of multiple nonmotor domains in cerebellar cortex (Guell et al. 2018a). The identification of two distinct nodes of DMN processing in right DN hints at the possibility that a multinodal representation of neural functions might also exist within DN.

Visual processing was identified as the third central component of DN functional neuroanatomy. It included connectivity mostly to association visual areas, and was segregated in

caudal and central-caudal components of left and right DN, respectively. Some previous reports are in agreement with a caudal distribution of visual processing in DN. Specifically, intracranial recording in monkeys revealed caudal DN neurons that responded specifically to "movement of the experimenter's arm or pieces of paper moved in particular parts of the visual field" that could not be attributed to eye movements (van Kan et al. 1993, p. 62), with previous investigations also reporting selective light stimulus-related neurons in caudal DN (Chapman et al. 1986) and anatomical connectivity from caudal DN to superior colliculi (May et al. 1990). More recently, task fMRI reports have identified visualspatial task activation in caudal DN bilaterally (Küper et al. 2011). It has also been demonstrated that nonhuman primate cortical visual inputs target specific territories of cerebellar cortex that then project to ventromedial aspects of DN (Xiong and Nagao 2002). Perhaps in agreement with the report of Xiong and colleagues, visual territories identified here in left and right DN encroached upon ventral DN surface.

### Dentate–Cerebral Cortical Functional Connectivity Weighted as a Factor of Dentate Functional Gradients

Calculation of dentate–cerebral cortical functional connectivity weighted as a factor of dentate functional gradients (Fig. 3) provided the following information. First, these analyses confirmed, using a method independent of clustering analyses, that DN functional gradient 1 captures a progression from functional territory 2 (salience/motor) to functional territory 3 (visual), and that DN functional gradient 2 captures a progression from functional territories 2 and 3 (salience/motor and visual) to functional territory 1 (default-mode). Second, DN functional gradients 1 and 2 visualized in this way revealed a progression similar to the two principal functional gradients of intracerebral cortical organization as reported in (Margulies et al. 2016). This observation is relevant as it contextualizes our results within a well-established division of functional neuroanatomy in cerebral cortex (Margulies et al. 2016). This observation may also provide a more nuanced reading of cerebral cortical functional gradients reported in (Margulies et al. 2016). Margulies and colleagues identified default-mode, primary motor/auditory, and primary visual processing as the three principal poles of human cerebral cortical functional neuroanatomy as indexed by resting-state fMRI. It is worth noting that salience processing territories such as Ins, dACC, and rMFG (described together in our analysis as a salience/motor network) also clustered together with motor regions in (Margulies et al. 2016). Similarly, VAAs which are consistently observed in our analyses of DN functional territory 3 were also part of the primary visual pole of cerebral cortical functional neuroanatomy in (Margulies et al. 2016) (see right column in Fig. 3, or figures in Margulies et al. 2016). In this way, the three principal poles of cerebral cortical functional neuroanatomy described by Margulies and colleagues (default-mode, primary motor/auditory, and primary visual) might be alternatively interpreted in line with our division of DN functional neuroanatomy as default-mode, motor/salience, and primary/association visual networks. Last, Figure 3 illustrates why some macroscale categories of brain function such as executive/frontoparietal network were not identified as separate functional territories in DN despite the fact that cerebellar links to executive function are well established in the animal anatomical literature (Dum and Strick 2003; Kelly and Strick 2003; Strick et al. 2009), consistently identified in human task-based (Stoodley and Schmahmann 2009; Stoodley et al. 2012; Keren-Happuch et al. 2014; Guell et al. 2018a; King et al. 2019) and resting-state neuroimaging investigations (Habas et al. 2009; O'Reilly et al. 2010; Buckner et al. 2011; Guell et al. 2018a; Marek et al. 2018), and a central component of the constellation of the cerebellar cognitive affective syndrome observed after damage to the cognitive cerebellum in the posterior lobe (Schmahmann and Sherman 1998; Schmahmann et al. 2009; Stoodley et al. 2016; Hoche et al. 2018). In Margulies et al. (2016), frontoparietal network was not located at any of the three poles of cerebral cortical functional organization (default-mode, motor/auditory/salience, and visual), despite being well-characterized as an independent component of human cerebral cortical functional neuroanatomy (e.g., Yeo et al. 2011). This observation indicated that frontoparietal network has a less unique resting-state functional connectivity signature when compared with default-mode, motor/salience, and visual processing networks. In the same way, frontoparietal territories in our analysis were not situated at any pole of DN functional gradient 1 or 2 (Fig. 3). This middle location of brain territories that are part of frontoparietal network in our DN functional gradient space (see Fig. 3A) explains the fact that frontoparietal network was not identified as an independent functional division of DN. Following the same logic as in Margulies et al. (2016), frontoparietal network representation in DN might have a functional connectivity signature that is not as unique as the functional connectivity signatures of default-motor, salience/-motor, and visual processing DN regions. Task-based analyses may allow a better characterization of specific functional networks that were not isolated by our data-driven resting-state parcellation.

### Relevance for Cerebellar Neuroscience, Neurology, and Psychiatry

Our results provide a systems-neuroscience substrate for cerebellar output to influence multiple broad categories of neural organization—namely, default-mode, attentional-motor, and visual. Brain networks such as salience and default-mode, here mapped to distinct DN territories for the first time, are central players in the evolving understanding of systems neuroscience in neurology and psychiatry. Identifying and mapping these macroscale networks in different brain territories is relevant for the characterization of functional and structural abnormalities in psychopathology (Palaniyappan and Liddle 2012; Whitfield--Gabrieli and Ford 2012; Darby et al. 2018), and necessary for the development of targeted brain stimulation interventions (Esterman et al. 2017). In the specific case of cerebellar cortex, damage to the cerebellar posterior lobe, which provides inputs to the DN, causes the cerebellar cognitive affective syndrome, characterized by deficits in executive, linguistic, visuospatial, and affective processing (Schmahmann and Sherman 1998; Schmahmann et al. 2009; Guell et al. 2015; Hoche et al. 2016, 2018; Stoodley et al. 2016). In addition, multiple studies have reported cerebellar cortical abnormalities in disorders such as Alzheimer's disease (Guo et al. 2016; Jacobs et al. 2018), schizophrenia (Moberget et al. 2018), and autism spectrum disorder (e.g., D'Mello and Stoodley 2015; Arnold Anteraper et al. 2019) (see also literature linking cerebellum to social cognition; e.g., Van Overwalle et al. 2014, 2015, 2019; Hoche et al. 2016; Guell et al. 2018a), and preliminary evidence suggests that cerebellar cortical stimulation might improve symptoms in these diseases (Demirtas-Tatlidede et al. 2010; Di Lorenzo et al. 2013; Tikka et al.

2015; Garg et al. 2016; Stoodley et al. 2017; Brady et al. 2019). The importance of our findings is thus underscored by the relevance of cerebellar cortex in neurology and psychiatry (Schmahmann et al. 2019), as the majority of fibers exiting the cerebellar cortex synapse in DN before reaching extracerebellar structures such as cerebral cortex.

A better understanding of DN functional organization is relevant for the characterization of cerebellar and cerebellar-linked neuropathology. DN parcellation results (Fig. 2A), made publicly available in our online repository, provide new scientific knowledge concerning the functional organization of human DN, and the first data-driven functional parcellation of human DN. The replication of these findings suggests that these parcellations are generalizable to independent studies. Classical reports demonstrated topography of DN histological changes following lesions to distinct territories of the cerebral hemispheres, dating as back as 1927 (as reported in Smyth 1941). More recent reports indicate that specific neurological symptoms in cerebellar disease may correlate with atrophy in specific locations within DN (Ilg et al. 2013). The present observations provide an opportunity for an improved topographical interpretation of the functional significance of these findings. Similarly, previous investigations in psychiatry have observed abnormalities in functional connectivity when using all combined territories of DN as a seed (Olivito et al. 2017). Our results provide a more precise method of DN seed selection that might improve the detection of DN functional connectivity abnormalities in patient populations.

## Limitations and Future Studies

Functional characterization of territories in DN was based on resting-state connectivity with cerebral cortex. While the connectivity patterns observed here corresponded to well-established brain networks, future investigations of task-based fMRI may provide an improved characterization of the functional contributions of each DN compartment. Task-based analyses might also allow a better characterization of specific functional networks that were not isolated by our data-driven resting-state parcellation. For example, task-based analyses might better characterize the topography of executive functional networks in human DN such as frontoparietal network, which is represented in cerebellar cortex (Buckner et al. 2011), but was not identified as a separate component in our analysis. Overlapping task-based activation maps with data-driven resting-state parcellations of human DN might also help to elucidate the origin of subdivisions identified in our analysis. For example, size or spatial distribution of specific functions in human DN as indexed by task fMRI might account for the inability of our analysis to identify these networks as separate functional territories.

DTI investigations of DN-cerebral connectivity (including both DN-thalamic and DN-cerebral cortical connectivity) might provide a complementary approach to the characterization of human DN neuroanatomy. Connections from DN to thalamus through the superior cerebellar peduncle (SCP) pose nontrivial methodological challenges to DTI analyses. Fibers in SCP are densely compact, an anatomical reality that complicates the attempt to determine the origin within the SCP of fibers arising from focal territories of the DN. Methodological approaches to address these challenges are starting to be developed, with current analyses still restricted to whole-DN masks as tractography seeds to analyze DN-cerebral connectivity (Granziera et al. 2009; Ji et al. 2019b). It is conceivable that DN subregions identified using alternative methods such as resting-state functional connectivity not affected by anatomical limitations such as SCP fiber density may facilitate the discovery of DTI-visible human anatomical tracts linking focal areas of DN to discrete regions of thalamus and cerebral cortex. Masks of DN functional territories publicly available in our online repository might be helpful in future DTI-focused neuroimaging analyses that explore this possibility.

While our analyses in adolescent and adult samples (Fig. 2B and **Supplementary Fig. 1**, respectively) indicate that DN functional subdivisions remain observable in these two age groups, it is possible that there are gradual subtle changes in these connectivity patterns that could be identified in analyses specifically examining age effects. While this analysis is beyond the scope of the present investigation, our DN parcellations that are publicly available may facilitate the investigation of this question in future studies. In the adult replication dataset, mPFC was not observed as part of DMN (see Supplementary Fig. 1). This observation raises the possibility that some functional aspects of DMN are more represented in DN than others, perhaps differently across age groups. Within DMN, mPFC may facilitate information manipulation during internally-oriented mentation (Buckner et al. 2008). Future studies may investigate whether specific nodes, and thus specific functional aspects, of DMN are over- or under-represented in DN.

Our investigation was focused on cerebral cortical patterns of connectivity, rather than connectivity from DN to cerebellar cortex or other subcortical structures such as thalamus. One methodological limitation of analyzing connectivity to cerebellar cortex is that functional connectivity clusters corresponding to within-DN connectivity may bleed into cerebellar cortex given the close proximity of the two structures. Bleeding from cerebellar cortex to DN would be most concerning if seeds were placed in DN to examine functional connectivity between DN and cerebellar cortex. This is because cluster-size statistical thresholding would facilitate the merging of separate DN and cerebellar cortical clusters into single clusters, blurring the boundaries between DN and cerebellar cortical anatomy. Our analyses were based on functional connectivity from DN to cerebral cortex, and therefore merging of clusters between DN and cerebellar cortex as a result of cluster-size thresholding was not an issue in our analyses. Partial volume effects in DN from surrounding structures (white matter, cerebellar cortex, fastigial, and interposed nuclei) are still a possibility; while these limitations are present in all neuroimaging experiments, we note that (i) 64Ch data used in the present study provides improved SNR and contributes to lower partial volume effects (Keil et al. 2013), (ii) DN-cerebral cortical connectivity data used to define the borders of DN functional territories was smoothed in cerebral cortex but not in DN or any of its neighbor structures; this approach minimizes partial volume effects from structures close to DN such as white matter, cerebellar cortex, fastigial, and interposed nuclei, while allowing an optimization of signal-to-noise in cerebral cortical data; and (iii) default-mode, motor-salience, and visual networks remained observable when using unsmoothed data in post hoc analyses to characterize the functional contributions of each DN functional territory (see **Supplementary Fig. 2**). Within other territories of subcortex, functional connectivity values are generally weaker as fMRI signal in the subcortex is not as robust as in the cerebral cortex. Possibly as a result of these limitations, our exploratory analyses in

cerebellar cortex and thalamus did not reveal functional connectivity maps from DN functional territories that remained observable in both the discovery and replication samples. A large and expanding body of evidence describing DN-thalamic and DN-cerebellar cortical relations indicates that our inability to detect replicable networks in these territories is almost certainly a measurement limitation. Anatomical tract tracing studies demonstrate topographically arranged projections to the DN from cerebellar cortex in rodents and monkeys (Lu et al. 2007; Hashimoto et al. 2010; Prevosto et al. 2010) (see Voogd 2014 for a review). In humans, DTI experiments also report a precise map of cerebellar cortical–DN connections (Steele et al. 2017), and these relationships are echoed in task-based analyses that describe simultaneous and nonoverlapping cerebellar cortical and DN activation in multiple motor and nonmotor domains (Küper et al. 2011, 2012, 2014; Thürling et al. 2011). DN ascending projections are directed to the cerebral cortex after an obligatory synapse in the thalamus; maps of cerebellar-thalamic connectivity can be reliably identified in anatomical studies in rats, primates, and other animals (Percheron et al. 1996; Dum and Strick 2003; Hintzen et al. 2018). Thalamic microstimulation in monkeys elicits motor responses in thalamic regions that receive cerebellar afferents (Vitek et al. 1996; Miall et al. 1998), and common networks in fMRI experiments in humans can be successfully identified in both cerebellar cortex and thalamus (Ji et al. 2019a). Mapping connectivity from DN to cerebellar cortex and thalamus is thus an important area of functional neuroanatomy that could be further explored in future investigations. Of note, a cerebellar cortical fractured somatotopy has been described at the submillimeter scale in rat (Shambes et al. 1978), cat (Kassel et al. 1984), oppossum (Welker and Shambes 1985), and galago (Wally et al. 1988). It is not clear whether fMRI can capture fractured somatotopy in cerebellar cortex. Neuroimaging studies discussing this possibility emphasize that the resolution needed to resolve fractured somatotopy is likely two orders of magnitude below the resolution of fMRI experiments, and conclude that there is a nonfractured somatotopy at a macroscopic level detected by fMRI that is in contrast with a fractured somatotopy at the submillimiter scale (Rijntjes et al. 1999; Van der Zwaag et al. 2013). It is not clear whether fractured topography exists also in nonmotor cerebellar territories; this intriguing question might be explored in future studies. In the context of the present investigation, it is possible that fractured cerebellar topography underlies, at least in part, our inability to observe reliable DN-cerebellar cortical functional relations. An additional contributing factor might be the fact that the same DN territory may receive projections from multiple territories of the cerebellar cortex (as indicated by rodent and primate anatomical studies; see Figure 5 in Voogd 2014).

Lastly, resting-state functional connectivity is inherently limited due to its correlational nature—a causal demonstration of human DN functional territories could be achieved with modulation/stimulation experiments. Recent developments utilizing these methods suggest that it might be possible in the near future to target specific subterritories in human DN noninvasively (Lee et al. 2015, 2016; Grossman et al. 2017; Folloni et al. 2019; Verhagen et al. 2019).

Our study reveals for the first time that DN subdivisions span a broad spectrum of human macroscale neural specialization categories, namely, default-mode, attentional-motor, and visual. This observation is consistent with the anatomical knowledge that large territories of cerebellar cortex project to DN. As cerebellar cortex contains representations of default-mode, attentional, and multiple unimodal domains, it is logical to detect a similar spectrum of functional diversity in DN. This reasoning leads us to hypothesize that a similar organization should be observable in analogous brain compartments—such as pontine nuclei, that are an obligatory relay of topographically arranged cerebral cortical projections reaching the cerebellar cortex (Schmahmann and Pandya 1995, 1997; Schmahmann 1996; Schmahmann et al. 2004a, 2004b), or inferior olivary nuclei, that send and receive projections to and from cerebellar nuclei in a topographically precise fashion (Holmes and Stewart 1908; Voogd et al. 2013). In this way, DN findings presented here unmask new predictions for basic human functional neuroanatomy of other largely unexplored brain territories.

## Supplementary Material

Supplementary material is available at *Cerebral Cortex* online.

## Funding

This work was supported in part by La Caixa Banking Foundation (100010434, LCF/BQ/AN15/10380048 to X.G.); the MGH Tosteson & Fund for Medical Discovery Award (to X.G.); US National Institutes of Health (NIH) grants 1U01NS104326-01 (to J.D.S.), 1R01NS080816-01A1 (to J.D.S.), U01MH108168 (to J.D.E.G. and S.W.G.), F32MH114525 (to N.A.H.), F32MH117933 (to A.M.D.), T32MH112510 (to R.R.R.), and F31HD086957 (to R.R.R.); the William and Flora Hewlett Foundation (4429) (to J.D.E.G.); the Simons Center for the Social Brain (postdoctoral fellowship to A.M.D.); the National Ataxia Foundation (to J.D.S.); the MINDlink foundation (to J.D.S.); and the Athinoula A. Martinos Imaging Center at the McGovern Institute for Brain Research at MIT.

## Notes

The authors thank Scott Marek for his help reviewing the literature regarding differences between adolescent and adult brain functional architecture; Viviana Siless, Anastasia Yendiki, Stefan Hofmann, Diego Pizzagalli, Randy Auerbach, and Aude Henin for their contributions to the U01MH108168 study; Yoon Ji Lee for technical assistance with data compilation; Drs Kennedy and Byrge from IU for their contributions to the ABIDE dataset; and Atsushi Takahashi for technical assistance regarding MRI sound measurements. *Conflict of Interest*: The authors declare no competing financial interests.

## References

Agcaoglu O, Miller R, Mayer AR, Hugdahl K, Calhoun VD. 2014. Lateralization of resting state networks and relationship to age and gender. *Neuroimage*. 104:310–325.

Albus K, Donate-Oliver F, Sanides D, Fries W. 1981. The distribution of pontine projection cells in visual and association cortex of the cat: an experimental study with horseradish peroxidase. *J Comp Neurol*. 201(2):175–189.

Amiez C, Petrides M. 2014. Neuroimaging evidence of the anatomo-functional organization of the human cingulate motor areas. *Cereb Cortex*. 24(3):563–578.

Arnold Anteraper S, Guell X, D'Mello A, Joshi N, Whitfield-Gabrieli S, Joshi G. 2019. Disrupted cerebro-cerebellar intrinsic functional connectivity in young adults with high-functioning autism spectrum disorder: a data-driven,

whole-brain, high temporal resolution fMRI study. *Brain Connect*. 9(1):48–59.
Ashburner J, Friston KJ. 2005. Unified segmentation. *Neuroimage*. 26(3):839–851.
Barch DM, Burgess GC, Harms MP, Petersen SE, Schlaggar BL, *et al*. 2013. Function in the human connectome: task-fMRI and individual differences in behavior. *Neuroimage*. 80: 169–189.
Behzadi Y, Restom K, Liau J, Liu TT. 2007. A component based noise correction method (CompCor) for BOLD and perfusion based fMRI. *Neuroimage*. 37(1):90–101.
Bernard JA, Peltier SJ, Benson BL, Wiggins JL, Jaeggi SM, *et al*. 2014. Dissociable functional networks of the human dentate nucleus. *Cereb Cortex*. 24(8):2151–2159.
Brady RO, Gonsalvez I, Lee I, Öngür D, Seidman LJ, *et al*. 2019. Cerebellar-prefrontal network connectivity and negative symptoms in schizophrenia. *Am J Psychiatry*. 176(7):512–520.
Brissenden JA, Somers DC. 2019. Cortico-cerebellar networks for visual attention and working memory. *Curr Opin Psychol*. 29:239–247.
Buckner RL, Andrews-Hanna JR, Schacter DL. 2008. The brain's default network: anatomy, function, and relevance to disease. *Ann N Y Acad Sci*. 1124:1–38.
Buckner RL, Krienen FM, Castellanos A, Diaz JC, Yeo BTT. 2011. The organization of the human cerebellum estimated by intrinsic functional connectivity. *J Neurophysiol*. 106(5):2322–2345.
Cabeza R, Ciaramelli E, Moscovitch M. 2012. Cognitive contributions of the ventral parietal cortex: an integrative theoretical account. *Trends Cogn Sci*. 16(6):338–52.
Cavada C, Goldman-Rakic PS. 1989a. Posterior parietal cortex in rhesus monkey: I. Parcellation of areas based on distinctive limbic and sensory corticocortical connections. *J Comp Neurol*. 287(4):393–421.
Cavada C, Goldman-Rakic PS. 1989b. Posterior parietal cortex in rhesus monkey: II. Evidence for segregated corticocortical networks linking sensory and limbic areas with the frontal lobe. *J Comp Neurol*. 287(4):422–445.
Chapman CE, Spidalieri G, Lamarre Y. 1986. Activity of dentate neurons during arm movements triggered by visual, auditory, and somesthetic stimuli in the monkey. *J Neurophysiol*. 55(2):203–226.
Chen AC, Oathes DJ, Chang C, Bradley T, Zhou Z-W, *et al*. 2013. Causal interactions between fronto-parietal central executive and default-mode networks in humans. *Proc Natl Acad Sci*. 110(49):19944–19949.
Choi EY, Yeo BTT, Buckner RL, Buckner RL. 2012. The organization of the human striatum estimated by intrinsic functional connectivity. *J Neurophysiol*. 108(8): 2242–2263.
Coifman RR, Lafon S, Lee AB, Maggioni M, Nadler B, *et al*. 2005. Geometric diffusions as a tool for harmonic analysis and structure definition of data: multiscale methods. *Proc Natl Acad Sci*. 102(21):7432–7437.
Corbetta M, Shulman GL. 2002. Control of goal-directed and stimulus-driven attention in the brain. *Nat Rev Neurosci*. 3(3):201–215.
D'Mello AM, Stoodley CJ. 2015. Cerebro-cerebellar circuits in autism spectrum disorder. *Front Neurosci*. 9:408.
Darby R, Joutsa J, Fox M. 2018. Network localization of heterogeneous neuroimaging findings. *Brain*. 142(1):70–79.
De Zeeuw CI, Hoogenraad CC, Koekkoek SKE, Ruigrok TJH, Galjart N, Simpson JI. 1998. Microcircuitry and function of the inferior olive. *Trends Neurosci*. 21(9):391–400.
Deen B, Pitskel NB, Pelphrey KA. 2011. Three systems of insular functional connectivity identified with cluster analysis. *Cereb Cortex*. 21(7):1498–1506.
Demirtas-Tatlidede A, Freitas C, Cromer JR, Safar L, Ongur D, *et al*. 2010. Safety and proof of principle study of cerebellar vermal theta burst stimulation in refractory schizophrenia. *Schizophr Res*. 124:91–100.
Di Lorenzo F, Martorana A, Ponzo V, Bonnì S, D'Angelo E, *et al*. 2013. Cerebellar theta burst stimulation modulates short latency afferent inhibition in Alzheimer's disease patients. *Front Aging Neurosci*. 5:2.
Di Martino A, Yan CG, Li Q, Denio E, Castellanos FX, *et al*. 2014. The autism brain imaging data exchange: towards a large-scale evaluation of the intrinsic brain architecture in autism. *Mol Psychiatry*. 19(6):659–667.
Diedrichsen J, Maderwald S, Küper M, Thürling M, Rabe K, *et al*. 2011. Imaging the deep cerebellar nuclei: a probabilistic atlas and normalization procedure. *Neuroimage*. 54(3):1786–1794.
Dietrichs E. 1981. The cerebellar corticonuclear and nucleocortical projections in the cat as studied with anterograde and retrograde transport of horseradish peroxidase - IV. The paraflocculus. *Exp Brain Res*. 44(3):235–242.
Dum RP, Strick PL. 2003. An unfolded map of the cerebellar dentate nucleus and its projections to the cerebral cortex. *J Neurophysiol*. 89(1):634–639.
Esterman M, Thai M, Okabe H, DeGutis J, Saad E, *et al*. 2017. Network-targeted cerebellar transcranial magnetic stimulation improves attentional control. *Neuroimage*. 156:190–198.
Folloni D, Verhagen L, Mars RB, Fouragnan E, Constans C, *et al*. 2019. Manipulation of subcortical and deep cortical activity in the primate brain using transcranial focused ultrasound stimulation. *Neuron*. 101(6):1109–1116.e5.
Fox MD, Corbetta M, Snyder AZ, Vincent JL, Raichle ME. 2006. Spontaneous neuronal activity distinguishes human dorsal and ventral attention systems. *Proc Natl Acad Sci*. 103(26):10046–10051.
Fox MD, Snyder AZ, Vincent JL, Corbetta M, Van Essen DC, Raichle ME. 2005. The human brain is intrinsically organized into dynamic, anticorrelated functional networks. *Proc Natl Acad Sci*. 102(27):9673–9678.
Fries W. 1990. Pontine projection from striate and prestriate visual cortex in the macaque monkey: an anterograde study. *Vis Neurosci*. 4(3):205–216.
Garg S, Sinha VK, Tikka SK, Mishra P, Goyal N. 2016. The efficacy of cerebellar vermal deep high frequency (theta range) repetitive transcranial magnetic stimulation (rTMS) in schizophrenia: a randomized rater blind-sham controlled study. *Psychiatry Res*. 243:413–420.
Goulden N, Khusnulina A, Davis NJ, Bracewell RM, Bokde AL, *et al*. 2014. The salience network is responsible for switching between the default mode network and the central executive network: replication from DCM. *Neuroimage*. 99:180–190.
Granziera C, Schmahmann JD, Hadjikhani N, Meyer H, Meuli R, *et al*. 2009. Diffusion spectrum imaging shows the structural basis of functional cerebellar circuits in the human cerebellum in vivo. *PLoS One*. 4(4):e5101.
Greicius MD, Krasnow B, Reiss AL, Menon V. 2003. Functional connectivity in the resting brain: a network analysis of the default mode hypothesis. *Proc Natl Acad Sci*. 100(1):253–258.

Grossman N, Bono D, Dedic N, Kodandaramaiah SB, Rudenko A, *et al*. 2017. Noninvasive deep brain stimulation via temporally interfering electric fields. *Cell*. 169(6):1029–1041.e16.

Guell X, Gabrieli JDE, Schmahmann JD. 2018a. Triple representation of language, working memory, social and emotion processing in the cerebellum: convergent evidence from task and seed-based resting-state fMRI analyses in a single large cohort. *Neuroimage*. 172:437–449.

Guell X, Hoche F, Schmahmann JD. 2015. Metalinguistic deficits in patients with cerebellar dysfunction: empirical support for the dysmetria of thought theory. *Cerebellum*. 14(1):50–58.

Guell X, Schmahmann J, Gabrieli J, Ghosh S. 2018b. Functional gradients of the cerebellum. *Elife*. 7:e36652.

Guo CC, Tan R, Hodges JR, Hu X, Sami S, Hornberger M. 2016. Network-selective vulnerability of the human cerebellum to Alzheimer's disease and frontotemporal dementia. *Brain*. 139(5):1527–1538.

Habas C, Kamdar N, Nguyen D, Prater K, Beckmann CF, *et al*. 2009. Distinct cerebellar contributions to intrinsic connectivity networks. *J Neurosci*. 29(26):8586–8594.

Haines DE, Dietrichs E. 2012. The cerebellum - structure and connections. In: Day BL, Lord SR, editors. *Handbook of clinical neurology*. Amsterdam, Netherlands: Elsevier, pp. 3–36.

Hashimoto M, Takahara D, Hirata Y, Inoue KI, Miyachi S, et al. 2010. Motor and non-motor projections from the cerebellum to rostrocaudally distinct sectors of the dorsal premotor cortex in macaques. *Eur J Neurosci*. 31(8):1402–13.

Hastie T, Tibshirani R, Friedman J. 2009. *The elements of statistical learning the elements of statistical learningdata mining, inference, and prediction*. 2nd ed. Berlin, Germany: Springer.

Hayden BY, Smith DV, Platt ML. 2009. Electrophysiological correlates of default-mode processing in macaque posterior cingulate cortex. *Proc Natl Acad Sci*. 106(14):5948–5953.

He SQ, Dum RP, Strick PL. 1995. Topographic organization of corticospinal projections from the frontal lobe: motor areas on the medial surface of the hemisphere. *J Neurosci*. 15:3284–3306.

Hintzen A, Pelzer EA, Tittgemeyer M. 2018. Thalamic interactions of cerebellum and basal ganglia. *Brain Struct Funct*. 223(2):569–587.

Hoche F, Guell X, Sherman JC, Vangel MG, Schmahmann JD. 2016. Cerebellar contribution to social cognition. *Cerebellum*. 15(6):732–743.

Hoche F, Guell X, Vangel M, Sherman J, Schmahmann J. 2018. The cerebellar cognitive affective/Schmahmann syndrome scale. *Brain*. 141(1):248–270.

Holmes G, Stewart G. 1908. One the connection of the inferior olives with the cerebellum in man. *Brain*. 31(1):125–137.

Hwang K, Bertolero MA, Liu WB, D'Esposito M. 2017. The human thalamus is an integrative hub for functional brain networks. *J Neurosci*. 37(23):5594–5607.

Ilg W, Christensen A, Mueller OM, Goericke SL, Giese MA, Timmann D. 2013. Effects of cerebellar lesions on working memory interacting with motor tasks of different complexities. *J Neurophysiol*. 110(10):2337–2349.

Jacobs HIL, Hopkins DA, Mayrhofer HC, Bruner E, Van Leeuwen FW, *et al*. 2018. The cerebellum in Alzheimer's disease: evaluating its role in cognitive decline. *Brain*. 141(1):37–47.

Ji JL, Spronk M, Kulkarni K, Repovš G, Anticevic A, Cole MW. 2019a. Mapping the human brain's cortical-subcortical functional network organization. *Neuroimage*. 185:35–57.

Ji Q, Edwards A, Glass JO, Brinkman TM, Patay Z, Reddick WE. 2019b. Measurement of projections between dentate nucleus and contralateral frontal cortex in human brain via diffusion tensor tractography. *Cerebellum*. 18(4):761–769.

Kassel J, Shambes GM, Welker W. 1984. Fractured cutaneous projections to the granule cell layer of the posterior cerebellar hemisphere of the domestic cat. *J Comp Neurol*. 225(3):458–68.

Keil B, Blau JN, Biber S, Hoecht P, Tountcheva V, *et al*. 2013. A 64-channel 3T array coil for accelerated brain MRI. *Magn Reson Med*. 70(1):248–258.

Kelly RM, Strick PL. 2003. Cerebellar loops with motor cortex and prefrontal cortex of a nonhuman primate. *J Neurosci*. 23(23):8432–8444.

Keren-Happuch E, Chen SHA, Ho MHR, Desmond JE. 2014. A meta-analysis of cerebellar contributions to higher cognition from PET and fMRI studies. *Hum Brain Mapp*. 35(2):593–615.

King M, Hernandez-Castillo CR, Poldrack RA, Ivry RB, Diedrichsen J. 2019. Functional boundaries in the human cerebellum revealed by a multi-domain task battery. *Nat Neurosci*. 22(8):1371–1378.

Küper M, Dimitrova A, Thürling M, Maderwald S, Roths J, *et al*. 2011. Evidence for a motor and a non-motor domain in the human dentate nucleus - an fMRI study. *Neuroimage*. 54(4):2612–2622.

Küper M, Thürling M, Stefanescu R, Maderwald S, Roths J, *et al*. 2012. Evidence for a motor somatotopy in the cerebellar dentate nucleus-an fMRI study in humans. *Hum Brain Mapp*. 33(11):2741–2749.

Küper M, Wünnemann MJS, Thürling M, Stefanescu RM, Maderwald S, *et al*. 2014. Activation of the cerebellar cortex and the dentate nucleus in a prism adaptation fMRI study. *Hum Brain Mapp*. 35(4):1574–1586.

Lee W, Kim HC, Jung Y, Chung YA, Song IU, *et al*. 2016. Transcranial focused ultrasound stimulation of human primary visual cortex. *Sci Rep*. 6(34026).

Lee W, Kim H, Jung Y, Song IU, Chung YA, Yoo SS. 2015. Image-guided transcranial focused ultrasound stimulates human primary somatosensory cortex. *Sci Rep*. 5:8743.

Loh KK, Hadj-Bouziane F, Petrides M, Procyk E, Amiez C. 2018. Rostro-caudal organization of connectivity between cingulate motor areas and lateral frontal regions. *Front Neurosci*. 11:753.

Lu X, Miyachi S, Ito Y, Nambu A, Takada M. 2007. Topographic distribution of output neurons in cerebellar nuclei and cortex to somatotopic map of primary motor cortex. *Eur J Neurosci*. 25(8):2374–82.

Lynch JC, Hoover JE, Strick PL. 1994. Input to the primate frontal eye field from the substantia nigra, superior colliculus, and dentate nucleus demonstrated by transneuronal transport. *Exp Brain Res*. 100(1):181–6.

Marek S, Hwang K, Foran W, Hallquist MN, Luna B. 2015. The contribution of network organization and integration to the development of cognitive control. *PLoS Biol*. 13(12):e1002328.

Marek S, Siegel JS, Gordon EM, Raut RV, Gratton C, *et al*. 2018. Spatial and temporal organization of the individual cerebellum. *Neuron*. 100:977–993.

Margulies DS, Ghosh SS, Goulas A, Falkiewicz M, Huntenburg JM, *et al*. 2016. Situating the default-mode network along a principal gradient of macroscale cortical organization. *Proc Natl Acad Sci*. 113(44):12574–12579.

Matano S. 2001. Brief communication: Proportions of the ventral half of the cerebellar dentate nucleus in humans and great apes. *Am. J. Phys. Anthropol*. 114(2):163–65.

May PJ, Hartwich-Young R, Nelson J, Sparks DL, Porter JD. 1990. Cerebellotectal pathways in the macaque: implications for collicular generation of saccades. *Neuroscience*. 36(2):305–324.

Mesulam M, Mufson EJ. 1982. Insula of the old world monkey. III: efferent cortical output and comments on function. *J Comp Neurol*. 212(1):38–52.

Mesulam MM. 1998. From sensation to cognition. *Brain*. 121(6):1013–1052.

Miall RC, Price S, Mason R, Passingham RE, Winter JL, Stein JF. 1998. Microstimulation of movements from cerebellar-receiving, but not pallidal-receiving areas of the macaque thalamus under ketamine anaesthesia. *Exp Brain Res*. 123(4):387–96.

Moberget T, Doan NT, Alnæs D, Kaufmann T, Córdova-Palomera A, *et al*. 2018. Cerebellar volume and cerebellocerebral structural covariance in schizophrenia: a multisite mega-analysis of 983 patients and 1349 healthy controls. *Mol Psychiatry*. 23(6):1512–1520.

Morecraft RJ, van Hoesen GW. 1992. Cingulate input to the primary and supplementary motor cortices in the rhesus monkey: evidence for somatotopy in areas 24c and 23c. *J Comp Neurol*. 322(4):471–489.

Mufson EJ, Mesulam MM. 1982. Insula of the old world monkey. II: afferent cortical input and comments on the claustrum. *J Comp Neurol*. 212(1):23–37.

Leiner HC, Leiner AL, Dow RS. 1991. The human cerebro-cerebellar system: its computing, cognitive, and language skills. *Behav. Brain Res*. 44(2):113–28.

O'Reilly JX, Beckmann CF, Tomassini V, Ramnani N, Johansen-Berg H. 2010. Distinct and overlapping functional zones in the cerebellum defined by resting state functional connectivity. *Cereb Cortex*. 20(4):953–965.

Olivito G, Clausi S, Laghi F, Tedesco AM, Baiocco R, *et al*. 2017. Resting-state functional connectivity changes between dentate nucleus and cortical social brain regions in autism spectrum disorders. *Cerebellum*. 16(2):283–292.

Palaniyappan L, Liddle PF. 2012. Does the salience network play a cardinal role in psychosis? An emerging hypothesis of insular dysfunction. *J Psychiatry Neurosci*. 37(1):17–27.

Pandya D, Yeterian E. 1985. Architecture and connections of cortical association areas. In: Peters A, Jones E, editors. *Association and auditory cortices. cerebral cortex, Vol 4*. Boston (MA): Springer, pp. 3–61.

Pedregosa F, Varoquaux G. 2011. Scikit-learn: machine learning in python. *J Mach Learn Res*. 12:2825–2830.

Percheron G, François C, Talbi B, Yelnik J, Fénelon G. 1996. The primate motor thalamus. *Brain Res Brain Res Rev*. 22(2):93–181.

Prevosto V, Graf W, Ugolini G. 2010. Cerebellar inputs to intraparietal cortex areas LIP and MIP: functional frameworks for adaptive control of eye movements, reaching, and arm/eye/-head movement coordination. *Cereb Cortex*. 20(1):214–28.

Price CJ. 2012. A review and synthesis of the first 20years of PET and fMRI studies of heard speech, spoken language and reading. *Neuroimage*. 62(2):816–847.

Rijntjes M, Buechel C, Kiebel S, Weiller C. 1999. Multiple somatotopic representations in the human cerebellum. *Neuroreport*. 10(17):3653–3658.

Schmahmann J, Guell X, Stoodley C, Halko M. 2019. The theory and neuroscience of cerebellar cognition. *Annu Rev Neurosci*. 42:337–364.

Schmahmann JD. 1996. From movement to thought: anatomic substrates of the cerebellar contribution to cognitive processing. *Hum Brain Mapp*. 4(3):174–198.

Schmahmann JD, Ko R, MacMore J. 2004a. The human basis pontis: motor syndromes and topographic organization. *Brain*. 127(6):1269–1291.

Schmahmann JD, MacMore J, Vangel M. 2009. Cerebellar stroke without motor deficit: clinical evidence for motor and non-motor domains within the human cerebellum. *Neuroscience*. 162(3):852–861.

Schmahmann JD, Pandya DN. 1992. Course of the fiber pathways to pons from parasensory association areas in the rhesus monkey. *J Comp Neurol*. 326(2):159–179.

Schmahmann JD, Pandya DN. 1993. Prelunate, occipitotemporal, and parahippocampal projections to the basis pontis in rhesus monkey. *J Comp Neurol*. 337:94–112.

Schmahmann JD, Pandya DN. 1995. Prefrontal cortex projections to the basilar pons in rhesus monkey: implications for the cerebellar contribution to higher function. *Neurosci Lett*. 199(3):175–178.

Schmahmann JD, Pandya DN. 1997. Anatomic organization of the basilar pontine projections from prefrontal cortices in rhesus monkey. *J Neurosci*. 17(1):438–458.

Schmahmann JD, Rosene DL, Pandya DN. 2004b. Motor projections to the basis pontis in rhesus monkey. *J Comp Neurol*. 478(3):248–268.

Schmahmann JD, Sherman JC. 1998. The cerebellar cognitive affective syndrome. *Brain*. 121(4):561–579.

Schurz M, Radua J, Aichhorn M, Richlan F, Perner J. 2014. Fractionating theory of mind: a meta-analysis of functional brain imaging studies. *Neurosci Biobehav Rev*. 42:9–34.

Seeley WW, Menon V, Schatzberg AF, Keller J, Glover GH, *et al*. 2007. Dissociable intrinsic connectivity networks for salience processing and executive control. *J Neurosci*. 27(9):2349–2356.

Selemon LD, Goldman-Rakic PS. 1988. Common cortical and subcortical targets of the dorsolateral prefrontal and posterior parietal cortices in the rhesus monkey: evidence for a distributed neural network subserving spatially guided behavior. *J Neurosci*. 8(11):4049–4068.

Setsompop K, Gagoski BA, Polimeni JR, Witzel T, Wedeen VJ, Wald LL. 2012. Blipped-controlled aliasing in parallel imaging for simultaneous multislice echo planar imaging with reduced g-factor penalty. *Magn Reson Med*. 67(5):1210–1224.

Shambes GM, Gibson JM, Welker W. 1978. Fractured somatotopy in granule cell tactile areas of rat cerebellar hemispheres revealed by micromapping. *Brain Behav Evol*. 15(2):94–140.

Smyth G. 1941. The significance of lesions in the dentate nuclei apparently consecutive to disease of the frontal lobes. *Brain*. 64(1):63–72.

Sridharan D, Levitin DJ, Menon V. 2008. A critical role for the right fronto-insular cortex in switching between central-executive and default-mode networks. *Proc Natl Acad Sci*. 105(34):12569–12574.

Steele CJ, Anwander A, Bazin PL, Trampel R, Schaefer A, *et al*. 2017. Human cerebellar sub-millimeter diffusion imaging reveals the motor and non-motor topography of the dentate nucleus. *Cereb Cortex*. 27(9):4537–4548.

Stephani C, Fernandez-Baca Vaca G, MacIunas R, Koubeissi M, Lüders HO. 2011. Functional neuroanatomy of the insular lobe. *Brain Struct Funct*. 216(2):137–149.

Stoodley CJ, D'Mello AM, Ellegood J, Jakkamsetti V, Liu P, *et al*. 2017. Altered cerebellar connectivity in autism and cerebellar-mediated rescue of autism-related behaviors in mice. *Nat Neurosci*. 20(12):1744–1751.

Stoodley CJ, MacMore JP, Makris N, Sherman JC, Schmahmann JD. 2016. Location of lesion determines motor vs. cognitive

consequences in patients with cerebellar stroke. *NeuroImage Clin*. 12:765–775.
Stoodley CJ, Schmahmann JD. 2009. Functional topography in the human cerebellum: a meta-analysis of neuroimaging studies. *Neuroimage*. 44(2):489–501.
Stoodley CJ, Valera EM, Schmahmann JD. 2012. Functional topography of the cerebellum for motor and cognitive tasks: an fMRI study. *Neuroimage*. 59(2):1560–1570.
Strick PL, Dum RP, Fiez JA. 2009. Cerebellum and nonmotor function. *Annu Rev Neurosci*. 32(1):413–434.
Thürling M, Küper M, Stefanescu R, Maderwald S, Gizewski ER, *et al*. 2011. Activation of the dentate nucleus in a verb generation task: a 7T MRI study. *Neuroimage*. 57(3):1184–1191.
Tikka SK, Garg S, Sinha VK, Nizamie SH, Goyal N. 2015. Resting state dense array gamma oscillatory activity as a response marker for cerebellar-repetitive transcranial magnetic stimulation (rTMS) in schizophrenia. *J ECT*. 31(4):258–262.
Uddin LQ. 2015. Salience processing and insular cortical function and dysfunction. *Nat Rev Neurosci*. 16(1):55–61.
Van der Zwaag W, Kusters R, Magill A, Gruetter R, Martuzzi R, *et al*. 2013. Digit somatotopy in the human cerebellum: a 7T fMRI study. *Neuroimage*. 67:354–62.
van Es DM, van der Zwaag W, Knapen T. 2019. Topographic maps of visual space in the human cerebellum. *Curr Biol*. 29(10):1689–1694.e3.
van Kan PL, Houk JC, Gibson AR. 1993. Output organization of intermediate cerebellum of the monkey. *J Neurophysiol*. 69(1):57–73.
Van Overwalle F. 2009. Social cognition and the brain: a meta-analysis. *Hum Brain Mapp*. 30(3):829–858.
Van Overwalle F, Baetens K. 2009. Understanding others' actions and goals by mirror and mentalizing systems: a meta-analysis. *Neuroimage*. 48(3):564–584.
Van Overwalle F, Baetens K, Mariën P, Vandekerckhove M. 2014. Social cognition and the cerebellum: a meta-analysis of over 350 fMRI studies. *Neuroimage*. 86:554–572.
Van Overwalle F, Baetens K, Mariën P, Vandekerckhove M. 2015. Cerebellar areas dedicated to social cognition? A comparison of meta-analytic and connectivity results. *Soc Neurosci*. 10(4):337–344.
Van Overwalle F, De Coninck S, Heleven E, Perrotta G, Ben TNO, *et al*. 2019. The role of the cerebellum in reconstructing social action sequences: a pilot study. *Soc Cogn Affect Neurosci*. 14(5):549–558.
Verhagen L, Gallea C, Folloni D, Constans C, Jensen D, *et al*. 2019. Offline impact of transcranial focused ultrasound on cortical activation in primates. *Elife*. e40541:8.
Vitek JL, Ashe J, Delong MR, Kaneoke Y. 1996. Microstimulation of primate motor thalamus: somatotopic organization and differential distribution of evoked motor responses among subnuclei. *J Neurophysiol*. 75(6):2486–95.
Voogd J. 2014. What we do not know about cerebellar systems neuroscience. *Front Syst Neurosci*. 8:227.
Voogd J, Shinoda Y, Ruigrok TJH, Sugihara I. 2013. Cerebellar nuclei and the inferior olivary nuclei: organization and connections. In: Manto M, Schmahmann J, Rossi F, Gruol D, Koibuchi N, editors. *Handbook of the cerebellum and cerebellar disorders*. Berlin, Germany: Springer, 377–436.
Wally W, Blair C, Shambes GM. 1988. Somatosensory projections to cerebellar granule cell layer of giant bushbaby, galago crassicaudatus. *Evol Brain Behav*. 31(3):150–60.
Welker W, Shambes GM. 1985. Tactile cutaneous representation in cerebellar granule cell layer of the opossum, *Didelphis virginiana*. *Evol Brain Behav*. 27(2):57–79.
Whitfield-Gabrieli S, Ford J. 2012. Default mode network activity and connectivity in psychopathology. *Annu Rev Clin Psychol*. 8:49–76.
Whitfield-Gabrieli S, Nieto-Castanon A. 2012. Conn: a functional connectivity toolbox for correlated and anticorrelated brain networks. *Brain Connect*. 2(3):125–141.
Xiong G, Nagao S. 2002. The lobulus petrosus of the paraflocculus relays cortical visual inputs to the posterior interposed and lateral cerebellar nuclei: an anterograde and retrograde tracing study in the monkey. *Exp Brain Res*. 147(2): 252–263.
Yeo B, Krienen FM, Sepulcre J, Sabuncu MR, Lashkari D, *et al*. 2011. The organization of the human cerebral cortex estimated by intrinsic functional connectivity. *J Neurophysiol*. 106(3):1125–1165.
Zhou Y, Friston KJ, Zeidman P, Chen J, Li S, Razi A. 2018. The hierarchical organization of the default, dorsal attention and salience networks in adolescents and young adults. *Cereb Cortex*. 28(2):726–737.